Supplemental Material: Inverted orbital polarization in strained correlated oxide films

Paul C. Rogge,[1] Robert J. Green,[2,3] Padraic Shafer,[4] Gilberto Fabbris,[5] Andi M. Barbour,[6] Benjamin M. Lefler,[1] Elke Arenholz,[4] Mark P. M. Dean,[5] and Steven J. May[1]

[1]*Department of Materials Science and Engineering, Drexel University, Philadelphia, Pennsylvania 19104, USA*
[2]*Stewart Blusson Quantum Matter Institute, University of British Columbia, Vancouver, British Columbia V6T 1Z4, Canada*
[3]*Department of Physics & Engineering Physics, University of Saskatchewan, Saskatoon, Saskatchewan S7N 5E2, Canada*
[4]*Advanced Light Source, Lawrence Berkeley National Laboratory, Berkeley, California 94720, USA*
[5]*Department of Condensed Matter Physics and Materials Science, Brookhaven National Laboratory, Upton, New York 11973, USA*
[6]*National Synchrotron Light Source II, Brookhaven National Laboratory, Upton, New York 11973, USA*

I. X-ray absorption experiment and additional data

The x-ray incident angle was 20° relative to the film plane and the polarization was controlled upstream. A geometric correction was applied to the absorption measured with photons polarized out of the film plane, I_π:

$$I_z = \frac{(I_\pi - I_x \sin^2(\theta))}{\cos^2(\theta)}, \tag{1}$$

where I_x is the absorption intensity measured with photons polarized parallel to the film plane. At least 12 scans of each polarization were performed for the Fe L-edge measurements ($680 - 750$ eV), and at least four scans for the O K-edge ($513 - 555$ eV). The spectra were normalized by setting the pre-edge intensity to zero by subtracting a line fit to the pre-edge, followed by setting the post-L_2 intensity to unity at 750 eV for the Fe scans and setting the maximum intensity to unity for the O scans. The Fe x-ray absorption and XLD of the additional samples are shown in Fig. 1, and the O K-edge prepeak XLD of the additional samples are shown in Fig. 2.

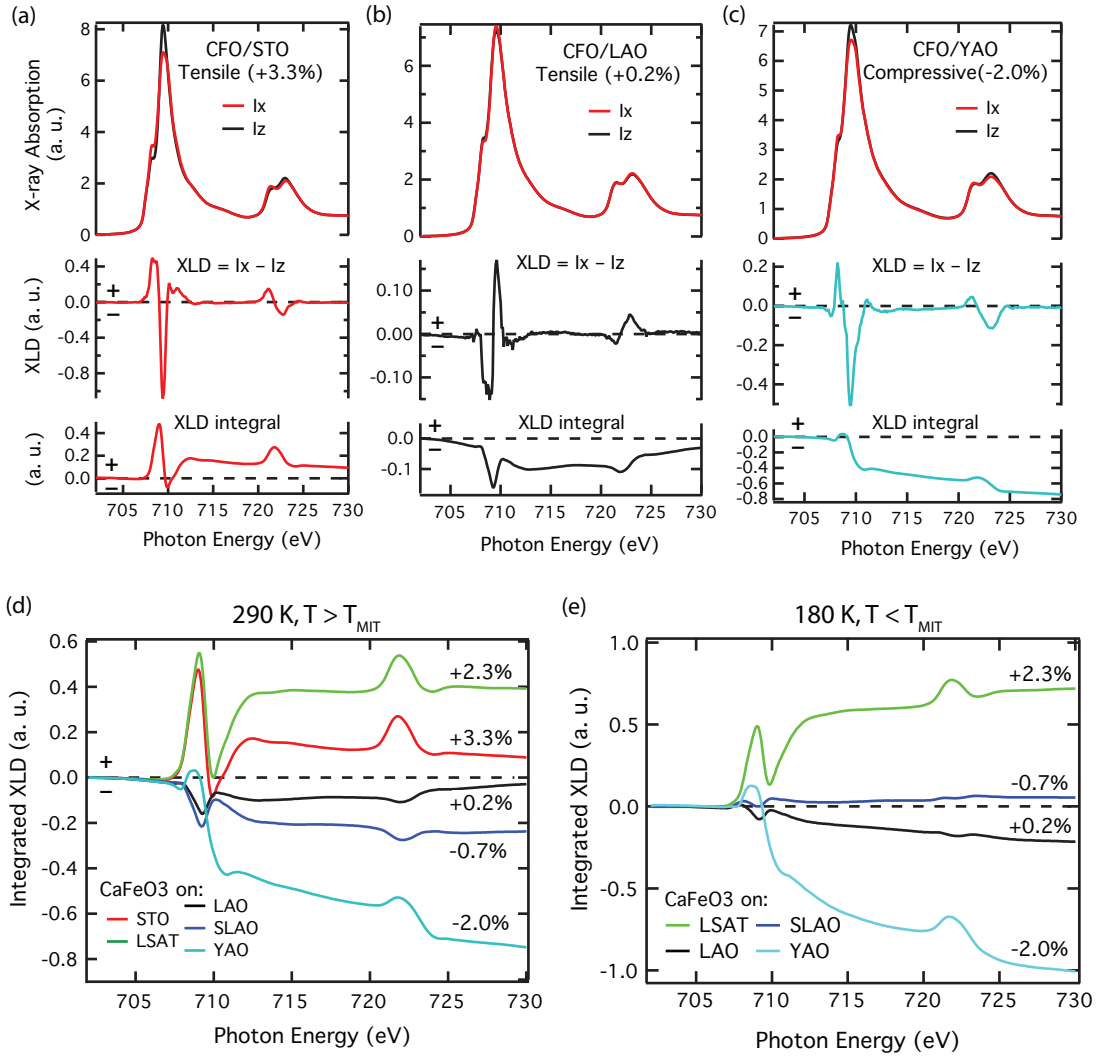

FIG. 1. Fe L-edge x-ray absorption data of additional $CaFeO_3$ films. Polarization-dependent x-ray absorption across the Fe L-edge for (a) tensile (+3.3%) $CaFeO_3$ on $SrTiO_3$, (b) relatively unstrained $CaFeO_3$ on $LaAlO_3$ (+0.2%), and (c) compressively strained (-2.0%) $CaFeO_3$ on $YAlO_3$. The resulting x-ray linear dichroism ($I_x - I_z$) and its integral are also shown. Measurements were made above $CaFeO_3$'s metal-insulator transition temperature (T_{MIT}). (d) The integrated XLD of all $CaFeO_3$ films for $T > T_{\mathrm{MIT}}$ (metallic) show consistent behavior: Tensile strained films have a positive XLD integral and compressively strained films have a negative XLD integral. (e) This behavior is maintained in the insulating state ($T < T_{\mathrm{MIT}}$). Data for $CaFeO_3$/STO sample was not obtained at 180 K.

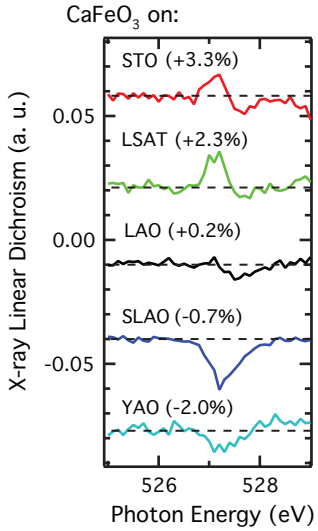

FIG. 2. O K-edge prepeak x-ray linear dichroism for all $CaFeO_3$ films measured by total fluorescence yield. The strain-dependent behavior is consistent with that seen for the Fe $3d$ e_g occupation.

II. Hole ratio derivation for $CaFeO_3$

Following Refs. [1, 2], the relative intensities for x, y, and z polarized light are given by

$$\begin{aligned} I_x &= \frac{1}{n}(\frac{1}{2}n_{xy} + \frac{1}{2}n_{xz} + \frac{1}{6}n_{z^2} + \frac{1}{2}n_{x^2-y^2}) \\ I_y &= \frac{1}{n}(\frac{1}{2}n_{xy} + \frac{1}{2}n_{yz} + \frac{1}{6}n_{z^2} + \frac{1}{2}n_{x^2-y^2}) \\ I_z &= \frac{1}{n}(\frac{1}{2}n_{xz} + \frac{1}{2}n_{yz} + \frac{2}{3}n_{z^2}) \end{aligned} \tag{2}$$

where I_j is the normalized intensity along direction j, n_i is the number of holes in orbital i, and n is the total number of holes. For high-spin $CaFeO_3$, the t_{2g} shell is half-full, and under moderate strains we assume negligible polarization of the t_{2g} orbital occupation, *i.e.*,

$$\begin{aligned} n_{xy} &= 1 \\ n_{xz} &= 1 \\ n_{yz} &= 1, \end{aligned} \tag{3}$$

where we leave the e_g occupation as unknown. This then gives

$$\frac{I_x}{I_z} = \frac{\frac{1}{2} + \frac{1}{2} + \frac{1}{6}n_{z^2} + \frac{1}{2}n_{x^2-y^2}}{\frac{1}{2} + \frac{1}{2} + \frac{2}{3}n_{z^2}} = \frac{6 + n_{z^2} + 3n_{x^2-y^2}}{6 + 4n_{z^2}}, \tag{4}$$

where $n_{x^2-y^2}$ and n_{z^2} are the number of holes in the $d_{x^2-y^2}$ and $d_{3z^2-r^2}$ orbitals, respectively. This equation can only be solved if the total e_g occupation is known. As discussed in the main manuscript, we estimate that the total e_g occupation for $CaFeO_3$ is 1.85.

III. Optimization of the ligand field model parameters

We employed a standard multiplet ligand field theory model using the code *Quanty* [3, 4], which computes the eigenstates and spectra using exact diagonalization. The model includes the Fe $3d$ shell, a ligand shell comprised of d-symmetry linear combinations of oxygen $2p$ orbitals, and the Fe core $2p$ shell (needed for the spectroscopy simulations). Parameters of the model include the local Fe Coulomb and exchange integrals (F^k_{dd}, F^k_{pd}, and G^k_{pd}), for which we use Hartree-Fock determined values [5] that are subsequently rescaled to account for atomic as well as solid state corrections using inter- and intra-shell rescaling factors κ_{dd} and κ_{pd}, respectively. We also include the Fe atomic $3d$ and $2p$ spin orbit interaction (66 meV and 8.199 eV, respectively). We further include the octahedral crystal field splitting $10Dq$, as well as the strain induced, tetragonal crystal field distortion Δ_{e_g} $\left(\equiv 2\Delta_{t_{2g}}\right)$. Also included are the charge transfer energy Δ as well as the monopole parts of the valence-valence and core-valence Coulomb interactions ($U_{dd} = 6$ eV and $U_{pd} = 8$ eV, respectively). Finally, hybridization between the Fe $3d$ and ligand orbitals is included via O_h symmetry hopping integrals V_{e_g} and $V_{t_{2g}}$ $\left(\equiv 0.58V_{e_g}\right)$ [6], and in the XAS final state the hopping integrals are rescaled by V_f to account for orbital contraction due to the core hole.

The parameters used to calculate the $CaFeO_3$ x-ray absorption spectra were optimized by comparing the calculated x-ray linear dichroism to the experimental data. A single model parameter was systematically varied and all 10 independent spectra (arising from orbital and spin degeneracies of the initial state as described in the main text) were calculated for each parameter setting. The resulting x-ray linear dichroism spectra from each data set were then used to obtain the best possible fit to the experimental spectrum, illustrated here using the $CaFeO_3$/LSAT sample. The parameter value that gave the best fit to experiment (lowest χ^2 value) was taken as the optimized value. After optimizing all six model parameters in this manner, this process was repeated until the optimized parameters converged. The final parameters are shown in Table I.

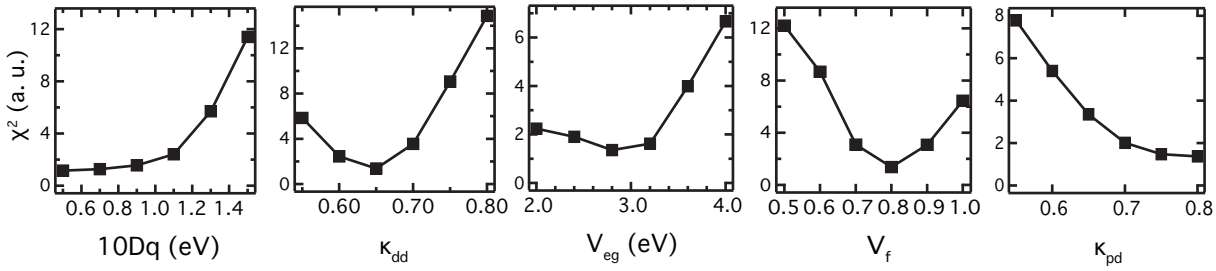

FIG. 3. Goodness of fit (χ^2) for the calculated x-ray linear dichroism as a function of crystal field ($10D_q$), intra-shell Coulomb interaction rescaling (κ_{dd}), hopping integrals (V_{e_g}, with $V_{t_{2g}} = 0.58V_{e_g}$ [6]), final state hopping rescaling (V_f), and inter-shell Coulomb and exchange interaction rescaling (κ_{pd}). The relevant set of 10 independent spectra was calculated for each parameter value and then the weights of each spectrum were fit to the experimental $CaFeO_3$/LSAT x-ray linear dichroism data to obtain the χ^2 value.

TABLE I. Optimized parameters for the ligand field simulations of the x-ray absorption and linear dichroism for $CaFeO_3$: Crystal field ($10D_q$), hopping (V_{eg}), final state hopping rescaling factor (V_f), intra-shell Coulomb interaction rescaling factor (κ_{dd}), inter-shell Coulomb and exchange interaction rescaling factor (κ_{pd}), and charge transfer energy (Δ).

Parameter	$10D_q$ (eV)	V_{eg} (eV)	V_f	κ_{dd}	κ_{pd}	Δ (eV)
Value	0.5	2.80	0.80	0.65	0.80	-2.0

IV. Breakdown of the J_z fits

Tables 2 and 3 show the breakdown of the fit of the calculated x-ray linear dichroism spectrum to the experimental $CaFeO_3$/LSAT and $CaFeO_3$/SLAO spectra, respectively. Under tensile strain, states having preferential $x^2 - y^2$ occupation are lower in energy than those having preferential $3z^2-r^2$ occupation, and their respective spin multiplicity derived spectra (labelled by J_z) are split in energy by a few meV due to the Fe 3d spin-orbit coupling. The resulting coefficient value (fit weight) and its 95% confidence interval are shown for the optimized fit. Although the relative J_z contributions do not follow a Boltzmann distribution [7], this is not unexpected given that a Boltzmann distribution would not reproduce the inverted orbital polarization. Moreover, small distortions of the local symmetry of the crystal field are expected to change the relative energy alignment of the J_z spectra, particularly given the small separation in energy of roughly 5 meV.

To determine the e_g orbital occupation, the weight of each J_z spectrum is multiplied by its electron occupation in the $x^2 - y^2$ and $3z^2 - r^2$ orbitals. These reported occupations are the electron count in the Fe 3d orbitals only and do not include the ligand hole count. The resulting values are then summed for $d_{x^2-y^2}$ and $d_{3z^2-r^2}$ in order to obtain the e_g electron occupation values.

TABLE II. J_z fit breakdown for $CaFeO_3$/LSAT, Δe_g = +40 meV.

J_z spectrum	Energy above ground state (meV)	Fit weight	±95% conf. int.	Weight (%)	95% conf. int. (%)	$x^2 - y^2$ occup.	$3z^2 - r^2$ occup.	Weight% *occup $x^2 - y^2$	Weight% *occup $3z^2 - r^2$
pref $3z^2 - r^2$, $J_z = 0$	23	3.06	0.57	18.8	3.5	0.71	1.14	0.13	0.21
pref $3z^2 - r^2$, $J_z = \pm1$	22	5.74	0.89	35.3	5.5	0.71	1.14	0.25	0.40
pref $3z^2 - r^2$, $J_z = \pm2$	18	0.00	0.36	0.0	2.2	0.71	1.14	0.00	0.00
pref $x^2 - y^2$, $J_z = \pm2$	5	4.26	0.46	26.2	2.8	1.14	0.71	0.30	0.19
pref $x^2 - y^2$, $J_z = \pm1$	2	1.06	0.67	6.5	4.1	1.14	0.71	0.07	0.05
pref $x^2 - y^2$, $J_z = 0$	0	2.15	0.54	13.2	3.3	1.14	0.71	0.15	0.09
Sum		16.27		100.0				0.91	0.94

TABLE III. J_z fit breakdown for $CaFeO_3$/SLAO, Δe_g = -30 meV.

J_z spectrum	Energy above ground state (meV)	Fit weight	±95% conf. int.	Weight (%)	95% conf. int. (%)	$x^2 - y^2$ occup.	$3z^2 - r^2$ occup.	Weight% *occup $x^2 - y^2$	Weight% *occup $3z^2 - r^2$
pref $x^2 - y^2$, $J_z = \pm2$	20	2.97	0.18	18.4	1.1	1.15	0.71	0.21	0.13
pref $x^2 - y^2$, $J_z = \pm1$	17	3.63	0.3	22.5	1.9	1.14	0.72	0.26	0.16
pref $x^2 - y^2$, $J_z = 0$	16	1.44	0.16	8.9	1.0	1.13	0.72	0.10	0.06
pref $3z^2 - r^2$, $J_z = 0$	7	1.62	0.24	10.1	1.5	0.71	1.14	0.07	0.11
pref $3z^2 - r^2$, $J_z = \pm1$	4	1.96	0.26	12.2	1.6	0.71	1.14	0.09	0.14
pref $3z^2 - r^2$, $J_z = \pm2$	0	4.49	0.22	27.9	1.4	0.71	1.14	0.20	0.32
Sum		16.11		100.0				0.93	0.93

V. Anisotropic band broadening scenarios

Bandwidth effects are illustrated in Fig. 4 for three scenarios: a less-than-half-filled band, a half-filled band, and a greater-than-half-filled band. In the simplest picture, the unstrained system has equal bandwidths in all three directions. Applying tensile strain ($\Delta e_g > 0$) lowers the $x^2 - y^2$ band in energy relative to the $3z^2 - r^2$ band and, as seen in Fig. 4(a), the $x^2 - y^2$ band is more occupied. For the less-than-half-filled band (Fig. 4(a)) and the half-filled band (Fig. 4(b)), adding in the tensile strain-induced anisotropic bandwidth effects, where the in-plane $x^2 - y^2$ band broadens and the out-of-plane $3z^2 - r^2$ band narrows, still results in $x^2 - y^2$ being more occupied and thus does not replicate our findings.

In contrast, for a greater-than-half-filled band the band broadening can result in an inverted orbital polarization. As seen in Fig. 4(c), band broadening results in the higher energy edge of the $x^2 - y^2$ band surpassing the $3z^2 - r^2$ band edge, and the $3z^2 - r^2$ band becomes more occupied than $x^2 - y^2$. From this simple illustration, an inverted orbital polarization can be expected when the net change in bandwidth is greater than the strain-induced Δe_g and the bands are more-than-half-filled.

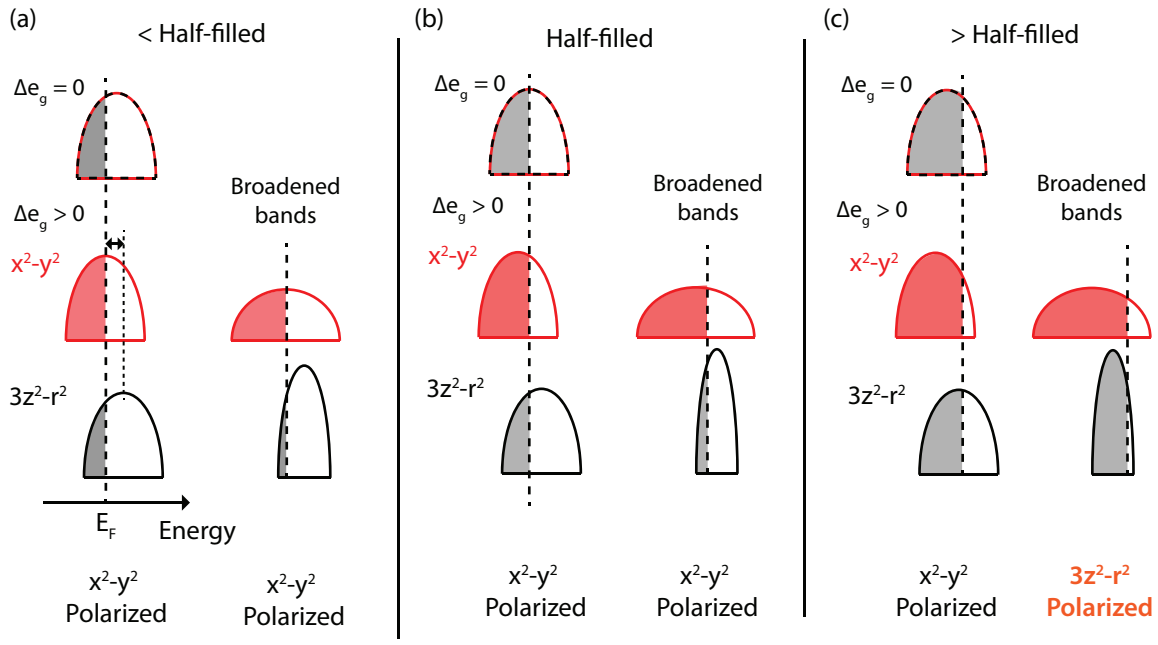

FIG. 4. Simplified schematic of the effect of changes in bandwidth on the resulting orbital polarization for a system under tensile strain ($\Delta e_g > 0$), which shifts the band center of masses about the unstrained center. Broadening of the in-plane band and narrowing of the out-of-plane band for the (a) less-than-half-filled band and (b) half-filled band results in the conventional preferential $x^2 - y^2$ orbital polarization. (c) For a band with greater than half-filling, the same broadening can result in an inverted orbital polarization with $3z^2 - r^2$ preferentially occupied.

[1] B. T. Thole, P. Carra, F. Sette, and G. van der Laan, Phys. Rev. Lett. **68**, 1943 (1992).
[2] M. W. Haverkort, *Spin and orbital degrees of freedom in transition metal oxides and oxide thin films studied by soft x-ray absorption spectroscopy*, Ph.D. thesis, University of Cologne (2005).
[3] M. W. Haverkort, M. Zwierzycki, and O. K. Andersen, Phys. Rev. B **85**, 165113 (2012).
[4] M. W. Haverkort *et al.*, `http://www.quanty.org`.
[5] R. D. Cowan, *The Theory of Atomic Structure and Spectra* (University of California Press, 1981).
[6] R. J. Green, M. W. Haverkort, and G. A. Sawatzky, Phys. Rev. B **94**, 195127 (2016).
[7] M. W. Haverkort, Z. Hu, A. Tanaka, G. Ghiringhelli, H. Roth, M. Cwik, T. Lorenz, C. Schüßler-Langeheine, S. V. Streltsov, A. S. Mylnikova, V. I. Anisimov, C. de Nadai, N. B. Brookes, H. H. Hsieh, H.-J. Lin, C. T. Chen, T. Mizokawa, Y. Taguchi, Y. Tokura, D. I. Khomskii, and L. H. Tjeng, Phys. Rev. Lett. **94**, 056401 (2005).